On the basin-scale detection and attribution of human-induced climate change in monsoon precipitation and streamflow

Arpita Mondal[1] and P. P. Mujumdar[1,2]

Received 30 September 2011; revised 30 August 2012; accepted 2 September 2012; published 9 October 2012.

[1] Detecting and quantifying the presence of human-induced climate change in regional hydrology is important for studying the impacts of such changes on the water resources systems as well as for reliable future projections and policy making for adaptation. In this article a formal fingerprint-based detection and attribution analysis has been attempted to study the changes in the observed monsoon precipitation and streamflow in the rain-fed Mahanadi River Basin in India, considering the variability across different climate models. This is achieved through the use of observations, several climate model runs, a principal component analysis and regression based statistical downscaling technique, and a Genetic Programming based rainfall-runoff model. It is found that the decreases in observed hydrological variables across the second half of the 20th century lie outside the range that is expected from natural internal variability of climate alone at 95% statistical confidence level, for most of the climate models considered. For several climate models, such changes are consistent with those expected from anthropogenic emissions of greenhouse gases. However, unequivocal attribution to human-induced climate change cannot be claimed across all the climate models and uncertainties in our detection procedure, arising out of various sources including the use of models, cannot be ruled out. Changes in solar irradiance and volcanic activities are considered as other plausible natural external causes of climate change. Time evolution of the anthropogenic climate change "signal" in the hydrological observations, above the natural internal climate variability "noise" shows that the detection of the signal is achieved earlier in streamflow as compared to precipitation for most of the climate models, suggesting larger impacts of human-induced climate change on streamflow than precipitation at the river basin scale.

Citation: Mondal, A., and P. P. Mujumdar (2012), On the basin-scale detection and attribution of human-induced climate change in monsoon precipitation and streamflow, *Water Resour. Res.*, *48*, W10520, doi:10.1029/2011WR011468.

1. Introduction

[2] Over the last two decades, there is an increasing interest in scientists, engineers and policy makers about how the climatic variables and associated natural resources and human systems are being affected by external forcings and whether such effects have surpassed the influence of natural internal variability of the climate. Detection and attribution (D&A) of human-induced climate change provide a formal tool to decipher the complex causes of climate change. The Intergovernmental Panel on Climate Change's (IPCC) good practice guidance paper on detection and attribution of climate change [Intergovernmental Panel on Climate Change, 2010] defines "detection" of climate change as "the process of demonstrating that climate or a system affected by climate has changed in some defined statistical sense, without providing a reason for that change," while "attribution" is defined as "the process of evaluating the relative contribution of multiple causal factors to a change or event with an assignment of statistical confidence." Regional D&A studies provide an insight to local changes in natural systems and may help in planning and developing robust adaptation strategies [*Hawkins and Sutton*, 2012].

[3] Formal detection and attribution have been previously used to investigate the nature of changes in various climatological variables such as air temperature [*Hegerl et al.*, 1996, *Allen and Stott*, 2003], ocean heat content [*Barnett et al.*, 2001], ocean circulation indices [*Santer et al.*, 1995], surface specific humidity [*Willett et al.*, 2007], tropospheric moisture content [*Santer et al.*, 2007], sea level pressure [*Gillett et al.*, 2003], continental river runoff [*Gedney et al.*, 2006], global land precipitation [*Zhang et al.*, 2007] and global precipitation extremes [*Min et al.*, 2011]. However, these studies deal with climatological or meteorological variables at the global or continental scale. Studies which have attempted to formally detect and attribute regional hydrometeorological changes to anthropogenic effects are rare. Regional-scale D&A analysis is more

[1]Department of Civil Engineering, Indian Institute of Science, Bangalore, India.
[2]Divecha Center for Climate Change, Indian Institute of Science, Bangalore, India.

Corresponding author: P. P. Mujumdar, Department of Civil Engineering, Indian Institute of Science, 560012 Bangalore India. (pradeep@civil.iisc.ernet.in)

0043-1397/12/2011WR011468

difficult because the detection of anthropogenic "signal" in natural internal climate variability "noise" is determined by the signal-to-noise ratio which is proportional to the spatial scale of analysis [*Karoly and Wu*, 2005; *Stott et al.*, 2010; *Hegerl and Zwiers*, 2011].

[4] *Timbal et al.* [2006] used the method of analogous synoptic situations to study the decrease in late 20th century rainfall in southwest Australia. *Wang et al.* [2009] quantified the effects of climate variations and human activities by a water balance model in the Chaobai River Basin in China. However, these two studies do not apply any formal D&A analysis to study the local hydrological changes.

[5] *Maurer et al.* [2007], *Bonfils et al.* [2008], *Pierce et al.* [2008], *Barnett et al.* [2008], *Hidalgo et al.* [2009] and *Pierce et al.* [2009] conducted a series of linked studies that performed formal regional D&A analysis on hydrological or hydrologically relevant meteorological variables for the Western United States. For largely snow-fed rivers in that mountainous region, these studies analyzed causes of larger spring runoff, rising winter and spring temperatures, earlier snowmelt and earlier streamflow center timings, which are direct implications of increasing greenhouse gases in the atmosphere and increasing global temperature.

[6] In the case of tropical river basins which are hugely dependent on monsoon rainfalls rather than snowmelt, it is necessary to study how monsoon precipitations or monsoon streamflows are affected by anthropogenic climate change. Monsoon precipitation and streamflow sustain a very large fraction of the total annual water resource for these river basins. Local hydrological impacts of climate change may not imply any obvious increasing or decreasing trend in tropical river basins, unlike in the case of snow-fed rivers. This motivates the current study which attempts to perform a formal D&A analysis to examine whether the observed trends in these hydrological variables lie statistically significantly outside the range that is expected from natural internal variability of climate alone and whether a signal of anthropogenic emissions is discernible in them.

[7] *Pierce et al.* [2009] applied multiple General Circulation Model (GCM) runs from the World Climate Research Programme's Coupled Model Intercomparison Project (WCRP/CMIP3) (see https://esg.llnl.gov:8443/about/ftp.do) for a regional D&A analysis considering hydrologically relevant temperature (January–February–March minimum near surface air temperature) as the detection variable. Their emphasis was more on the construction and application of performance metrics to assess GCM performances in simulating regional climate with respect to the D&A analysis.

[8] In this study, we attempt to detect and attribute anthropogenic climate change as well as study the time evolution of the signal-to-noise ratio for both precipitation and streamflow accounting for the variability across the different climate models of the WCRP/CMIP3. For each of the GCMs considered, we try to find answers to questions such as when is a change in hydrology above natural internal climate variability observed, and how much of the observed change is actually due to anthropogenic climate change.

[9] Thus, the objective of the study is to assess whether or to what extent the trends in observed monsoon precipitation or streamflow are likely to be resulting from the natural internal variability of climate alone or can be explained by external forcings. The effects of internal climate variability and external anthropogenic or solar and/or volcanic activities are estimated from statistically downscaled river basin–scale hydrological variables using corresponding large-scale climate variables from long, preindustrial control runs, or anthropogenically forced 20th century runs, or solar and/or volcanically forced historical runs, respectively, from each climate model.

[10] The standard "fingerprint" based D&A analysis has been applied (section 2), and the tropical rain-fed Mahanadi River flowing through the coastal region of Orissa in India is chosen as the case study for application (section 3). The results are discussed in section 4 and summarized in section 5. The principal component analysis and linear regression based statistical downscaling technique is described in details in Appendix A. For each of the climate model runs, a Genetic Programming (GP) based monthly rainfall-runoff model has been used to generate corresponding streamflows from precipitation. This GP-based rainfall-runoff model is explained in Appendix B.

2. Fingerprint-Based Detection and Attribution Methodology for River Basin–Scale Hydrology

[11] In the recent past, pattern-based "fingerprint" method of detection and attribution of human-induced climate change has been increasingly used as the foremost rigorous tool for assessing the complex causes of climate change [*Hasselmann*, 1979; *Hegerl et al.*, 1996; *Allen and Tett*, 1999; *Barnett et al.*, 2001]. The fingerprint defines the direction in which the human-induced signal is expected to lie [*Santer et al.*, 1995]. Fingerprint approaches reduce the detection problem to a univariate or low-dimensional problem in the detection variable [*Hegerl et al.*, 1996]. In this low-dimensional space, the human-induced climate change "signal" in the observations and the natural internal climate variability "noise" are statistically contrasted, and the detected vector is further compared with the vector obtained from the expected climate change pattern. Per *Barnett et al.* [2001, 2008], in this study the signal strength (S) is defined as the least squares linear trend of the hydrological vector projected into the fingerprint for each of the climate runs year by year. Thus, S is defined as

$$S = \text{trend}\,[F(\text{x}).D(x,t)], \tag{1}$$

where $F(x)$ is the signal fingerprint, $D(x,t)$ indicates the monsoon precipitation or streamflow time (t) series at the different locations (x), observed or downscaled from an ensemble model run and "trend" denotes least squares linear trend of the year by year dot product between $F(x)$ and $D(x,t)$. $D(x,t)$ series are standardized by removing time means and dividing by the standard deviations. A single spatial fingerprint, $F(x)$, from a GCM is defined as the leading Empirical Orthogonal Function (EOF) of the anthropogenically forced ensemble-averaged time series of monsoon precipitation or streamflow at the different locations for that GCM. For detection, it is examined how similar the observed changes in the monsoon precipitation or streamflow in the river basin are to the fingerprint. Also, the likelihood that a signal of the observed strength could have occurred by chance in the preindustrial control runs is thereafter calculated.

Estimation of internal climate variability "noise" from preindustrial control runs is a standard procedure when sufficiently long observational data sets uncontaminated by the searched-for signal is not available [*Jones and Hegerl*, 1998; *Barnett et al.*, 2001, 2005]. For attribution of the detected changes, it is needed to then test the hypothesis that the trends of the anthropogenically forced runs are consistent with the trends in the observations and that these signs are dissimilar to the solar and/or volcanically forced runs.

[12] The detectability over time for both monsoon precipitation and streamflow are assessed by the method of determining the earliest year in which human-induced climate change is detected over the natural variability, following *Santer et al.* [1995, 2007]. Starting from the commencing year of the observations of precipitation and streamflow, trends for increasingly longer intervals of time are calculated both for observed series and that from control runs. For each GCM, the year by year projections of the observational and the control runs standardized anomaly data onto the fingerprint yield the signal and noise time series $Z(t)$ and $N(t)$, respectively. Thus, for a hydrologic variable (i.e., monsoon precipitation or streamflow) for a GCM,

$$Z(t) = F(x).D_{obs}(x,t), \tag{2}$$

$$N(t) = F(x).D_{control}(x,t), \tag{3}$$

where $D_{obs}(x,t)$ and $D_{control}(x,t)$ are the $D(x,t)$ time series of equation (1) corresponding to observations and the control run, respectively. It may be noted that $N(t)$ is typically of much longer length compared to $Z(t)$. Least squares linear trends of increasing length L ($L = 10, 11, 12, \ldots$, to no. of years of observation) are fitted to $Z(t)$ and nonoverlapping L-length segments of the $N(t)$ time series. Thus, following *Santer et al.* [1995], if there are m nonoverlapping L-length segments in $N(t)$, with slopes $\beta(c)$, $c = 1, 2, \ldots, m$, the standard error of the linear trend, that is, the noise ε, is given by

$$\varepsilon = \left[\frac{1}{m-1}\sum_{c=1}^{m}\beta(c)^{2}\right]^{\frac{1}{2}}, \tag{4}$$

where the mean of $\beta(c)$ in the noise distribution is assumed to be zero.

[13] Detection is said to be achieved when the ratio of the linear observed signal trend (S_{obs}) to the noise ε (that is, the signal-to-noise ratio) stays at or above a stipulated significance threshold of 5% or 10%.

[14] It is to be noted that the optimization of the detection process to increase the signal-to-noise ratio is not performed here, since it requires a part of the control runs data to be used for optimization, which is not allowed to be used again for detection. This study focuses on river basin–scale detection and attribution of human-induced changes in hydrological variables for different climate models of the WCRP/CMIP3. While analyzing the evolution of the anthropogenic climate change signal using noise from individual model runs, losing a part of the control runs data for optimization might leave us with too few data to convincingly conclude about detection. Moreover, the exclusion of the optimization process makes our results rather conservative since the accentuation of the signal-to-noise ratio is likely to make detection all the more distinct and achieved earlier in time [*Santer et al.*, 1995, 2007].

3. Case Study Application

[15] The detection and attribution analysis of anthropogenic climate change in river basin–scale monsoon precipitation and streamflow is applied to the Mahanadi river basin in Orissa, India. Monsoon (total rainfall from June to September in a calendar year) precipitation at the eight locations in the basin (shown in Figure 1) and the corresponding streamflow of the river at the Hirakud Reservoir (shown in Figure 1) are the variables for which the analysis is performed. Studies have already been reported on assessment of impacts of climate change in the precipitation and streamflow in this region [e.g., *Ghosh and Mujumdar*, 2007, 2008; *Raje and Mujumdar*, 2009, 2010]. However, whether a human-induced climate change signal is indeed discernible in the hydrological observations of this river basin for the recent past needs to be assessed.

[16] The Mahanadi river basin is situated in eastern India between 19°20′ N and 23°35′ N latitude 80°30′ E and 86°50′ E longitude, and it flows eastward through most of the state of Chhattisgarh, much of Orissa, and portions of Jharkhand and drains into the Bay of Bengal. The river drains an area of 141,600 km^2 and is of utmost importance in the eastern part of India, both in terms of agriculture and the population base it supports. Being situated in a coastal region, climate change is quite likely to affect the hydrology of this river basin [*Raje and Mujumdar*, 2009]. Moreover, there have been reported increase of hydrologic extremes in the recent past and the increase in temperature in this region is 1.1°C/century, whereas the average increase for the whole country is about 0.4°C/century [*Rao and Kumar*, 1992; *Rao*, 1995].

[17] In most parts of India a significant portion of the total annual rainfall is received during the short span of summer monsoon. The summer monsoon rainfall over the Mahanadi basin occurs mostly due to low-pressure systems (LPSs) developing over the Bay of Bengal. *Mohapatra and Mohanty* [2006] have studied the role of LPSs on spatial and temporal variability of summer monsoon rainfall over Orissa. Orissa state, a meteorological subdivision of India, receives about 116.7 cm of rainfall during the southwest monsoon season (June–September). This is about 80% of the annual rainfall over Orissa [*Parthasarathy et al.*, 1995]. Therefore the monsoon rainfall at each of the eight rainfall locations is chosen as the first hydrological variable on which detection and attribution analysis is performed. Gridded observed monthly precipitation data for years 1951–1999 at 1° latitude by 1° longitude grid, interpolated from station data, are obtained from the India Meteorological Department (IMD). Figure 2 shows the time series of the observed monsoon precipitation at the eight locations from 1951–1999. A significant decreasing trend is found at 95% confidence level by the nonparametric Mann–Kendall test at locations 1, 5, 6, and 7. All the other locations show statistically insignificant trends. Very weak increasing trends are found in locations 3 and 4. In general, observed monsoon precipitation is found to decrease in the river basin.

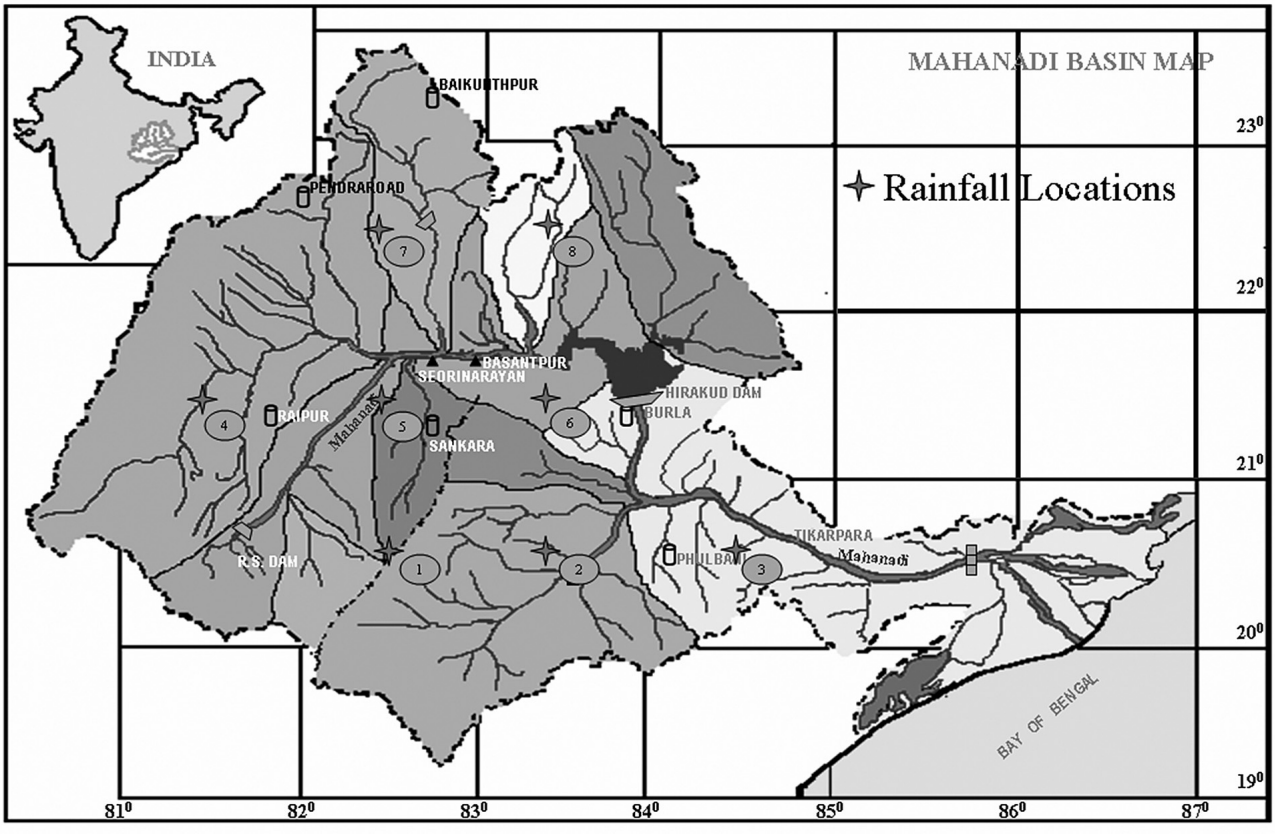

Figure 1. Mahanadi River Basin with the eight precipitation locations and the location of the Hirakud Dam [from *Raje and Mujumdar*, 2009].

[18] The Mahanadi River being mostly rain-fed, a large fraction of the total annual streamflow results during the summer monsoon, which is stored in the Hirakud Reservoir to meet the demands during the year. Absence of a major control structure upstream lets us treat the inflows to the Hirakud Reservoir as naturalized streamflows in the river. Observed monthly inflows are obtained from the Dept of Irrigation, Government of Orissa [*Patri*, 1993]. Figure 3 shows the time series of the observed monsoon streamflow of Mahanadi at Hirakud from 1959–1993.

[19] The observed monsoon streamflow also shows a significant decreasing trend at 90% confidence level by the nonparametric Mann–Kendall test. Significant decreases in both the monsoon precipitation and streamflow suggest that there have been major changes in the hydrology of the region. If such changes are due to natural variability of climate, the hydrological cycle is expected to revert back to its previous state with time [*Barnett et al.*, 2008]. However, if a human-induced climate change signal is indeed discernible in the observed decreases, modifications in water policies become indispensable for sustainable management of water resources in the river basin. Hence, a formal D&A analysis to detect and attribute human-induced climate change in the monsoon precipitation and streamflow in the river basin is required. To achieve this, the fingerprint-based detection method described in section 2 has been employed, along with several climate model simulations (including control runs and runs that are forced by anthropogenic emissions or solar and/or volcanic forcings), a statistical downscaling procedure to get the precipitations for each climate model simulation and a GP based rainfall-runoff model for generation of streamflows. As an example, the step-by-step procedure to get the observed signal strength (S_{obs}) for both precipitation and streamflow is shown in Figure 4. In order to get the signal strength for any other model run (say, segments from the control run, or any other run forced by an external forcing), the $D(x,t)$ series for precipitation and streamflow have to be simply replaced by the downscaled precipitation from that model run and the corresponding GP generated streamflow, respectively. The details of the elements used in the D&A analysis are discussed in the following sections.

3.1. Climate Models and Data

[20] The WCRP/CMIP3 archive has climate data simulated by 23 climate models by 15 modeling groups from across the world, in support of the Fourth Assessment Report of the Intergovernmental Panel on Climate Change (IPCC AR4). Since the purpose of this study is to demonstrate D&A analysis results across different climate models, 14 out of these 23 climate models are chosen as they have data available for all the four predictors for the downscaling model (described in section 3.2), over the region of interest, not only for the 20th century experiments, but also for the preindustrial control runs. The details of the models and simulations used in this study are indicated in Table 1. The control runs include only natural internal variability of climate (i.e., no external forcings), whereas the different

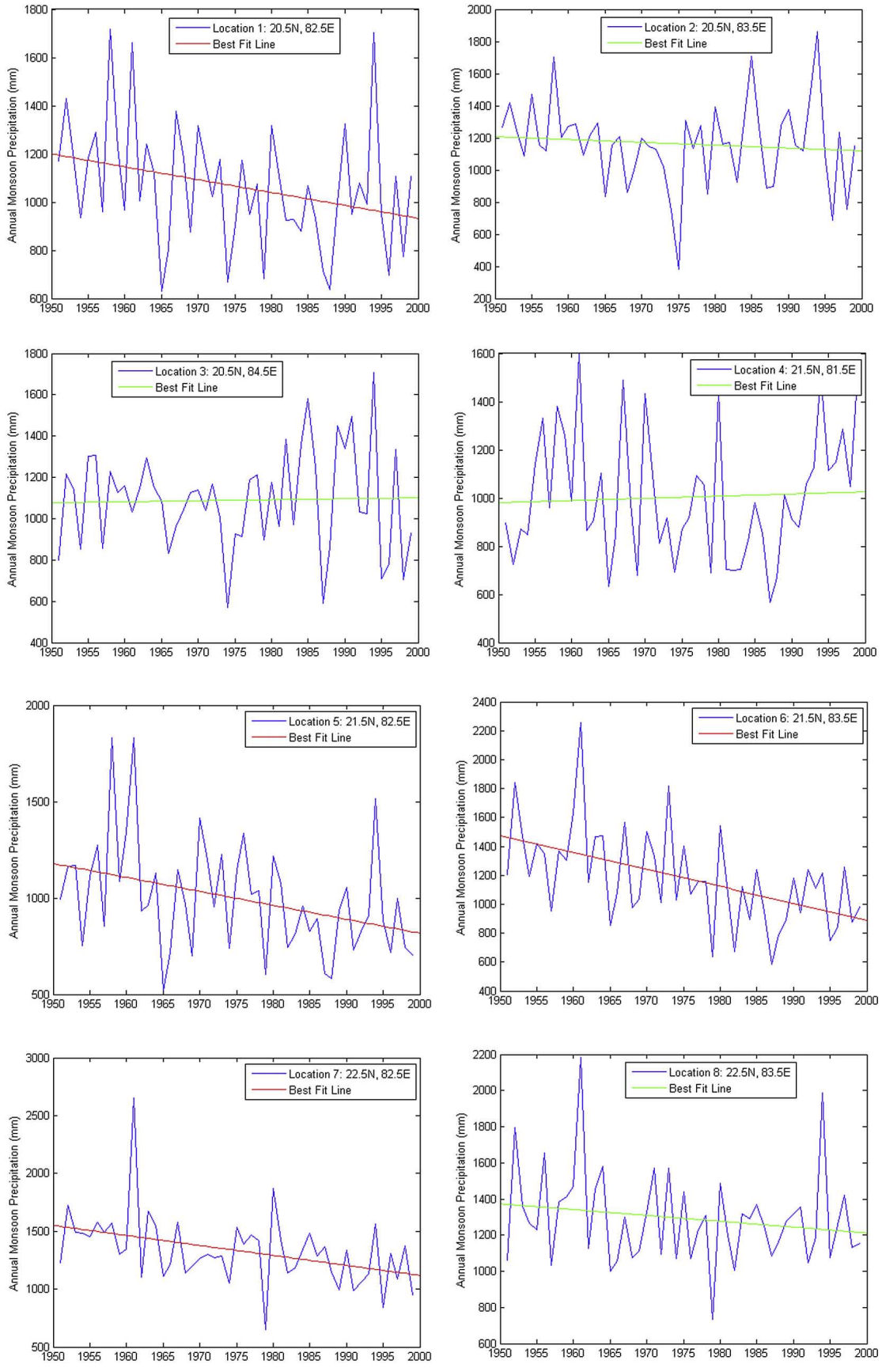

Figure 2. Observed monsoon precipitation at the eight locations. The best fit lines are also shown. Monsoon precipitation at stations 1, 5, 6, and 7 have statistically significant trends at 95% confidence level.

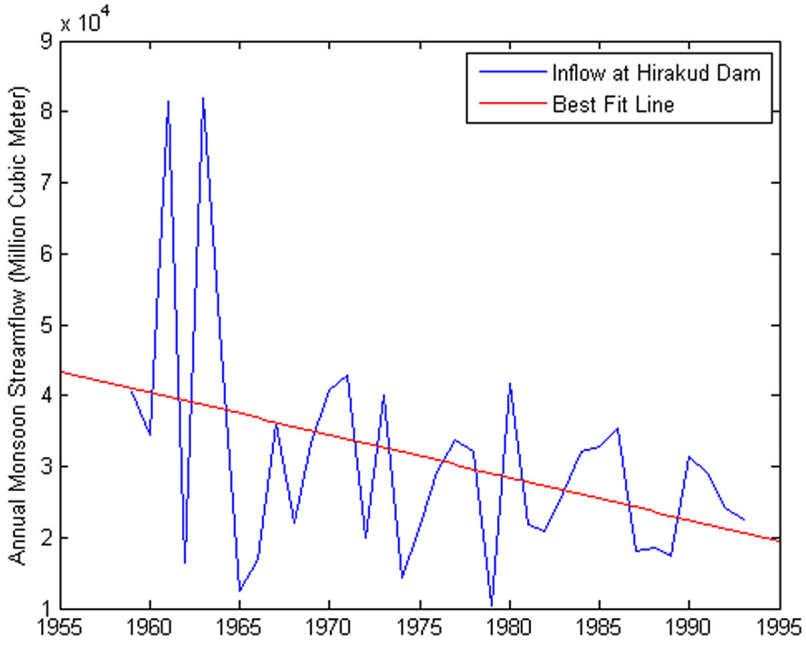

Figure 3. Observed monsoon streamflow in the Mahanadi River at the Hirakud Dam.

anthropogenically forced climate model runs include different combinations of natural and anthropogenic forcings. Four realizations (B06.66, B06.67, B06.68, B06.68) of the Parallel Climate Model (PCM2.1) forced with both solar and volcanic forcings, three realizations (B06.74, B06.75, B06.76) forced with only solar forcing and three realizations (B06.78, B06.79, B06.81) forced with only volcanic forcing, depending on availability of predictor data set, are

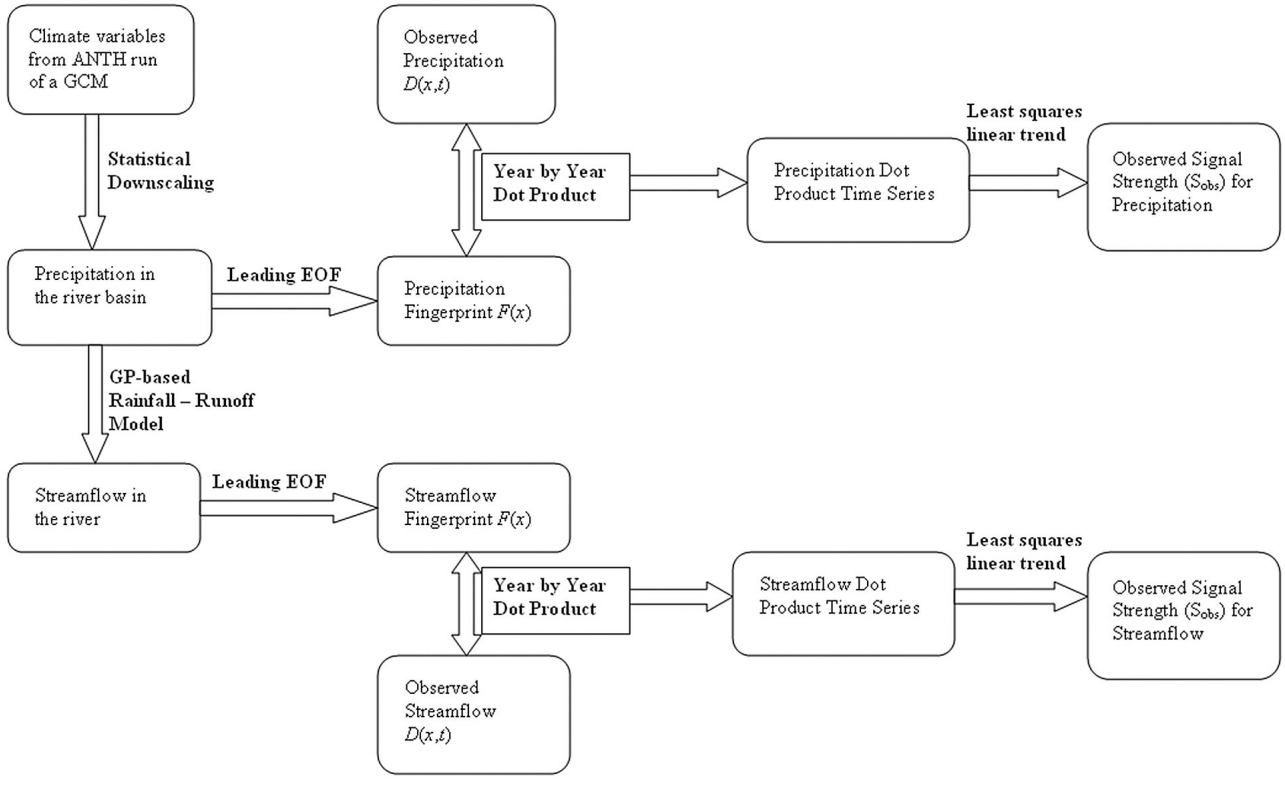

Figure 4. Step-by-step procedure for getting the observed signal strength (S_{obs}), for precipitation and streamflow. In order to obtain the signal strengths corresponding to a climate model run, the precipitation $D(x,t)$ is simply replaced with the statistically downscaled precipitation from that model run and the streamflow $D(x,t)$ is replaced with the corresponding GP generated streamflow.

Table 1. Details of the Climate Model Runs Used in This Study

Name of the Model Run	Model	Origin	No. of Years of Data Used
CONTROLbccr	BBCR-BCM2.0	Bjerknes Center for Climate Research, Norway	250
ANTHbccr	BBCR-BCM2.0	Bjerknes Center for Climate Research, Norway	1 × 49
CONTROLcgcm_t47	CCCma-CGCM3.1(T47)	Canadian Centre for Climate Modeling and Analysis, Canada	1001
ANTHcgcm_t47	CCCma-CGCM3.1(T47)	Canadian Centre for Climate Modeling and Analysis, Canada	5 × 49
CONTROLcgcm_t63	CCCma-CGCM3.1(T63)	Canadian Centre for Climate Modeling and Analysis, Canada	300
ANTHcgcm_t63	CCCma-CGCM3.1(T63)	Canadian Centre for Climate Modeling and Analysis, Canada	1 × 49
CONTROLcnrm	CNRM-CM3	Meteo-France/Centre National de Recherches Meteorologiques, France	500
ANTHcnrm	CNRM-CM3	Meteo-France/Centre National de Recherches Meteorologiques, France	1 × 49
CONTROLcsiro_mk3_0	CSIRO-Mk3.0	Commonwealth Scientific and Industrial Research Organization, Australia	380
ANTHcsiro_mk3_0	CSIRO-Mk3.0	Commonwealth Scientific and Industrial Research Organization, Australia	2 × 49
CONTROLcsiro_mk3_5	CSIRO-Mk3.5	Commonwealth Scientific and Industrial Research Organization, Australia	330
ANTHcsiro_mk3_5	CSIRO-Mk3.5	Commonwealth Scientific and Industrial Research Organization, Australia	3 × 49
CONTROLfgoals	IAP-FGOALS-g1.0	Institute for Atmospheric Physics, China	3 × 350
ANTHfgoals	IAP-FGOALS-g1.0	Institute for Atmospheric Physics, China	3 × 49
CONTROLinmcm	INM-CM3.0	Institute for Numerical Mathematics, Russia	330
ANTHinmcm	INM-CM3.0	Institute for Numerical Mathematics, Russia	1 × 49
CONTROLipsl	IPSL-CM4	Institute Pierre Simon Laplace, France	500
ANTHipsl	IPSL-CM4	Institute Pierre Simon Laplace, France	1 × 49
CONTROLmpi_echam5	ECHAM5/MPI-OM	Max-Planck Institute for Meteorology, Germany	506
ANTHmpi_echam5	ECHAM5/MPI-OM	Max-Planck Institute for Meteorology, Germany	3 × 49
CONTROLmri_cgcm	MRI-CGCM2.3.2a	Meteorological Research Institute, Japan	350
ANTHmri_cgcm	MRI-CGCM2.3.2a	Meteorological Research Institute, Japan	5 × 49
CONTROLpcm	PCM2.1	National Center for Atmospheric Research, USA	749
ANTHpcm	PCM2.1	National Center for Atmospheric Research, USA	6 × 49
SOLVOLpcm	PCM2.1	National Center for Atmospheric Research, USA	4 × 49
SOLpcm	PCM2.1	National Center for Atmospheric Research, USA	3 × 49
VOLpcm	PCM2.1	National Center for Atmospheric Research, USA	3 × 49
CONTROLhadcm3	UKMO-HadCM3	Hadley Center for Climate Prediction and Research, UK	341
ANTHhadcm3	UKMO-HadCM3	Hadley Center for Climate Prediction and Research, UK	2 × 49
CONTROLhadgem1	UKMO-HadGEM1	Hadley Center for Climate Prediction and Research, UK	240
ANTHhadgem1	UKMO-HadGEM1	Hadley Center for Climate Prediction and Research, UK	2 × 49

used to test whether the natural external effects can explain the observed changes in hydrology. Realizations with these natural external forcings alone are not available for any other GCM in the WCRP/CMIP3 database. Apart from the control runs, for all other GCM runs, climate model data from 1951–1999, corresponding to the period of observed hydrologic data, are collected from the WCRP/CMIP3 archive. The number of years of available control runs data varies across different GCMs, as shown in the last column of Table 1.

3.2. Downscaling Methodology

[21] The climate data from each realization of the GCMs, as mentioned in Table 1, are statistically downscaled to get the river basin–scale precipitation corresponding to them. A principle component analysis and simple linear regression based downscaling method taking seasonality into consideration is employed here, following *Ghosh and Mujumdar* [2006]. Near surface air temperature, mean sea level pressure, specific humidity at 850 hPa and geopotential height at 500 hPa are selected as predictors for precipitation in the downscaling model. Details of the downscaling method are given in Appendix A. The R values of the final regression models at the eight locations (1 to 8) are found to be 0.892, 0.906, 0.873, 0.898, 0.879, 0.922, 0.896 and 0.943, respectively. Overfitting is avoided by removing insignificant regression coefficients as found using the t-statistic.

[22] Additionally, a principal component analysis and artificial neural networks (ANN) based downscaling methodology is also employed. Several recent studies have used ANN as a statistical downscaling model to assess hydrological impacts of climate change [e.g., *Crane and Hewitson*, 1998; *Wilby et al.*, 1998; *Cavazos and Hewitson*, 2005]. In our opinion, linear regression and ANN form the two extremes in representing the predictor-predictand relationship which is the core of the statistical downscaling procedure, one being linear and the other being essentially nonlinear in nature. However, since no significant differences in the detection and attribution results are noticed by varying the downscaling model, the results shown here are those using only the linear regression based downscaling model. Use of any other statistical downscaling technique is unlikely to vary the results of the D&A analysis.

[23] It is to be noted, however, that the structure of the downscaling model is constant over all the scenarios of climate used in this study—the long preindustrial control runs as well as the externally forced historical runs. Stationarity assumption is a long-standing and well-recognized limitation of statistical downscaling [*Ghosh and Mujumdar*, 2006, 2008] and presently there is no other known alternative with respect to statistical downscaling that can be used here for obtaining rainfall corresponding to the different GCM runs.

3.3. Generation of Streamflows Corresponding to Different GCM Runs

[24] In order to generate streamflows corresponding to long preindustrial control runs or historical externally forced runs a GP-based rainfall-runoff model is employed. The statistically downscaled monthly precipitations from the climate model runs are used as input to the GP-based rainfall-runoff model. Monsoon streamflow in a year for each run is thereafter calculated from the monthly streamflow series.

[25] In the recent past, GP has been increasingly used to model the rainfall-runoff process [*Savic et al.*, 1999; *Whigham and Crapper*, 2001; *Muttil and Liong*, 2001; *Liong et al.*, 2002; *Dorado et al.*, 2003; *Babovic and Keijzer*, 2006; *Kashid et al.*, 2010; *Rodriquez-Vázquez et al.*, 2012] and has been shown to be a viable alternative to traditional rainfall-runoff models. This is particularly important for data scarce regions such as the Indian river basins, for which applications of a physically based hydrological model might be infeasible. Moreover, GP has the advantage of providing inherent functional input-output relationships as compared to traditional black box models, which can offer some possible interpretations to the underlying process [*Jayawardena et al.*, 2005].

[26] The rainfall-runoff model is calibrated using the observed monthly rainfall from July 1958 to June 1984 at locations 4 to 8 (since they are the ones contributing directly to the Mahanadi streamflow at Hirakud) as input, and the observed monthly inflows to the Hirakud reservoir as the target output. The weights of the rainfalls at each of these stations are implicitly learnt by the GP model; for example, rainfall at a station not contributing significantly to the streamflow at Hirakud is expected to have a low weight in the final GP model. The model does lead to negligibly small negative flows which are replaced by zero in our analysis. The data from July 1984 to June 1993 has been used for testing. Figure 5 shows the training and testing results of the rainfall-runoff model. The R values obtained for training and testing are 0.89 and 0.64, respectively. Methodological details of the GP-based rainfall-runoff model are described in Appendix B.

[27] The GP-based rainfall-runoff model is capable of learning and implicitly simulating the intermediate processes that convert rainfall into runoff. The structure and parameters of the GP-based rainfall-runoff model can be related to actual causal physical hydrological processes, following some recent studies which attempt to extract hydrological knowledge from artificial neural network model parameters [*Jain and Kumar*, 2009; *Sudheer and Jain*, 2009; *Jain et al.*, 2008]. However, this paradigm is out of scope of our present study since our primary focus remains on the D&A analysis. A more rigorous approach of generating the streamflows would be to consider all the influencing climate variables like temperature, humidity and wind speed that affect the intermediate processes in the conversion of rainfall to runoff in the streamflow generation process.

[28] It is to be also noted that the GP-based rainfall-runoff model structure, and hence the streamflow generating mechanism is assumed to be constant for generation of streamflows corresponding to all the scenarios—the long preindustrial control runs or the historical externally (naturally or anthropogenically) forced runs of climate models. Nonetheless, even if the computational GP-based rainfall-runoff model is replaced by a perfectly calibrated physically based distributed hydrological model like the Variable Infiltration Capacity (VIC) or the Soil and Water Assessment Tool (SWAT) or the Hydrologic Engineering Center's Hydrologic Modeling System (HEC-HMS), the results of the D&A analysis are unlikely to vary since the structure and parameters of these physically based models are also assumed to be constant for runoff generation corresponding to the preindustrial or historical climate model

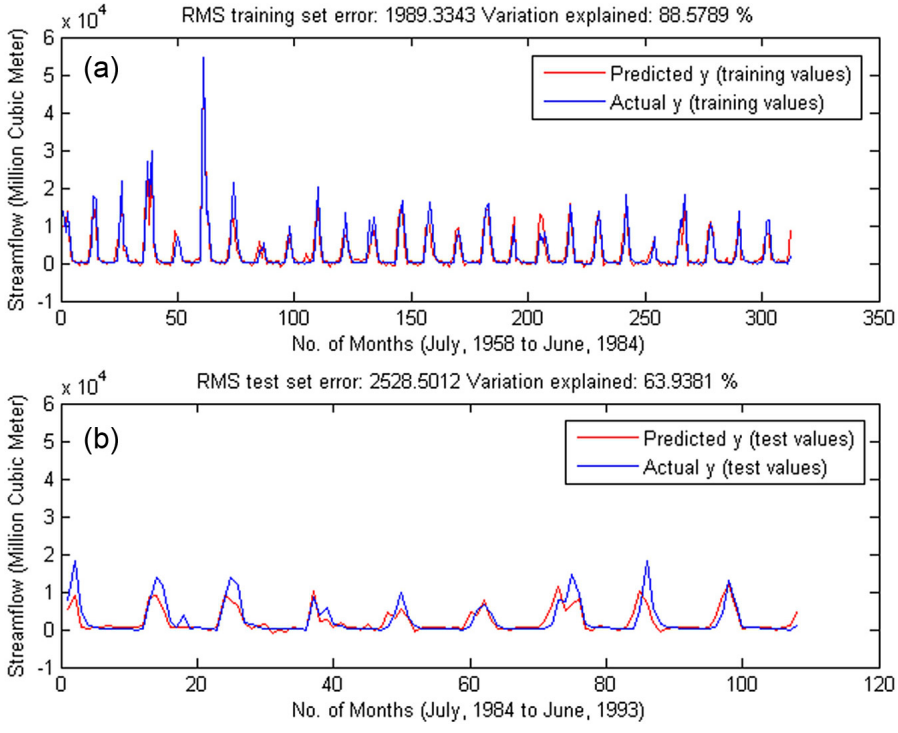

Figure 5. Performance of the GP-based rainfall-runoff model for (a) training and (b) testing periods. The subzero GP-simulated flow values, which are negligibly small in number and magnitude, are replaced by 0 for subsequent analysis.

runs [*Hidalgo et al.*, 2009]. The GP-based rainfall-runoff model can hence replace a perfectly calibrated physically based hydrological model. It can also be noted that the mapping between rainfall and runoff is highly complex and nonlinear since the model is calibrated with observed precipitation and streamflow data and conversion of observed rainfall to observed streamflows involve complex intermediate processes like evapotranspiration, infiltration, etc. Hence, even if the generated streamflows corresponding to all historical GCM runs are thus deterministically determined, the trends or variabilities in the generated streamflows would not be the same as the trends or variabilities of the rainfall used to generate them.

3.4. Calculation of Signal Strengths

[29] The statistically downscaled monsoon precipitations from the anthropogenically forced (ANTH) runs of the different GCMs at all the eight locations are expressed as anomalies with respect to the means calculated over the entire 49 years observation period, and thereafter standardized by division with the corresponding standard deviations. The single spatial precipitation fingerprint corresponding to each GCM is defined as the leading empirical orthogonal function (EOF) of the ensemble-averaged eight precipitation time series. Ensemble averaging and use of the leading EOF are both noise reduction techniques [*Santer et al.*, 1995; *Bonfils et al.*, 2008]. The projections of the observational, or downscaled data from preindustrial control runs of the GCMs or the anthropogenically or naturally forced runs of the GCMs on the fingerprint are used for the detection and attribution analysis. Thus, each location is weighted depending on how much it participates in the estimated anthropogenic signal. In general it is found that the EOF that comprises the fingerprint for each GCM, explains 70% or more of the total variance in the data set corresponding to the GCM.

[30] Figure 6 shows the fingerprints derived from the ensemble-averaged anthropogenically forced runs of the different GCMs for monsoon precipitation. For streamflow, since runoff at only one outlet for the single river is under consideration, the fingerprint is unity and does not define any spatial pattern. It can be observed from Figure 6 that the fingerprint is a monopole in sign across all the locations for all the GCMs. Also, fingerprints from the different GCMs are very similar despite their differences in external forcings. It is interesting to examine whether or not this leads to similar results in the D&A analysis. The multimodel ensemble-averaged fingerprint is also shown in Figure 6. Following the method given in *Santer et al.* [2007], the hydrological time series are first averaged across an individual model's 20th century realizations (where multiple realizations are available), and then the average across models is taken. The observed monsoon precipitations or the downscaled monsoon precipitations from the various climate model runs, and the corresponding streamflows are also standardized before the fingerprint is projected onto them to get the corresponding signal strength (S) values.

4. Results and Discussions

[31] The resulting detection plots for monsoon precipitation and streamflow are given in Figure 7 and Figure 8, respectively. The observed signal strengths, along with their 95% confidence intervals, calculated using different fingerprints from different GCMs are very similar. Considering fingerprints from all the GCMs, the observed signal strength for monsoon precipitation, for example, lies in the range [0.0439 ± 0.001]. The observed signal strength for monsoon streamflow is 0.0384 and it does not vary with different GCM fingerprints since the fingerprint for one streamflow location defines no spatial pattern. Hence, only the observed signal strengths considering multimodel ensemble-averaged

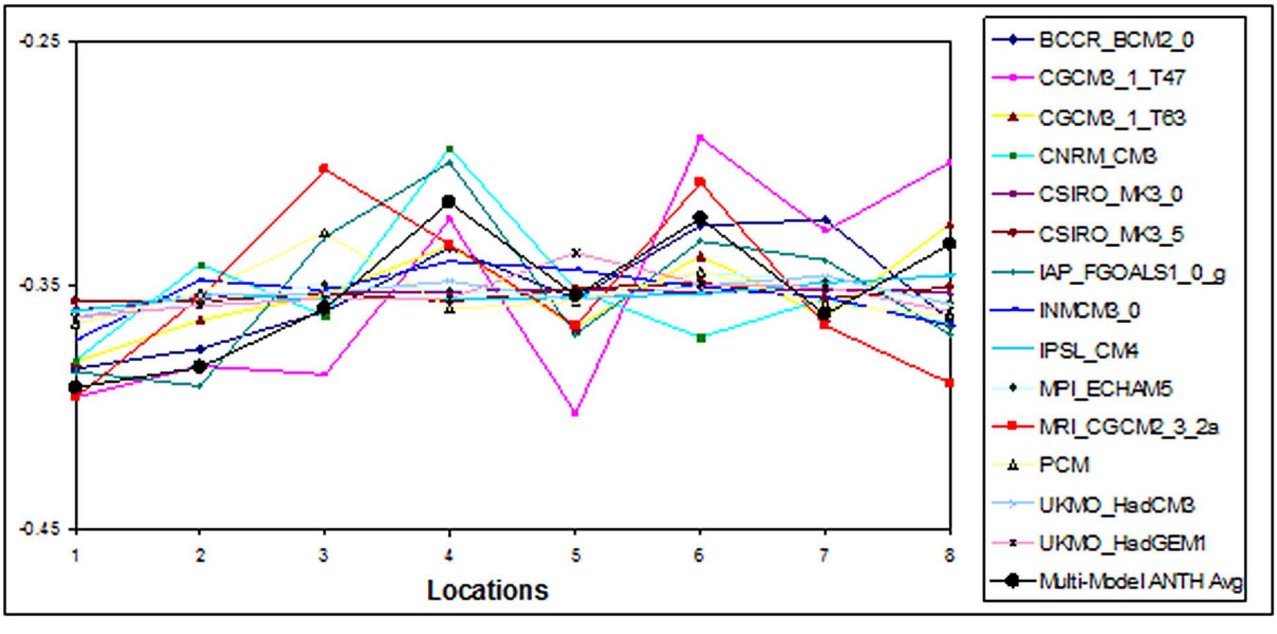

Figure 6. Fingerprints (Leading EOF loadings) from the anthropogenically forced runs of the different GCMs for monsoon precipitation. The multimodel ensemble-averaged ANTH fingerprint is shown in black. The locations follow no ordering and the EOF loadings at the locations are not connected.

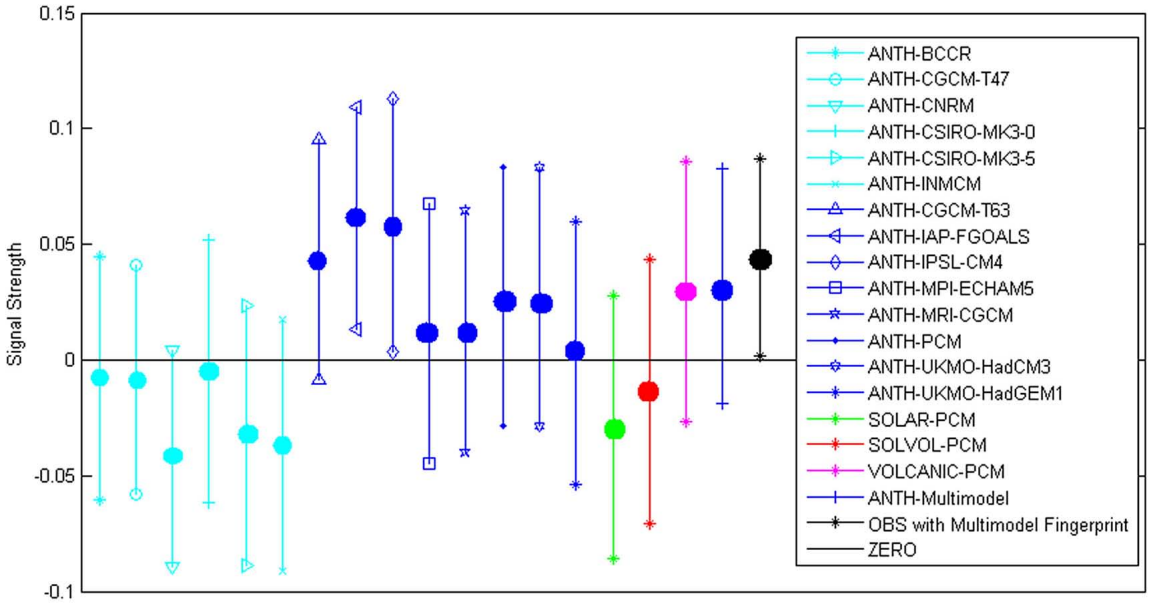

Figure 7. Detection plot for monsoon precipitation. The ensemble-averaged signal strengths (S values) from each model run (dots) and their 95% confidence intervals (bars) are shown. The observed signal strength (S_{obs}) with its 95% confidence interval, considering the multimodel ensemble-averaged ANTH fingerprint is shown in black. The GCMs for which the ANTH signal strength is inconsistent in sign with the observed signal strength are marked in cyan and those for which the ANTH signal strength is consistent with the observed signal strength are marked in blue.

fingerprint is shown in Figure 7 and Figure 8. The observations show a positive signal, which does not include zero at 95% statistical confidence level. The percentile ranks with respect to the noise distribution for the observed signal strength as well as the ensemble-averaged signal strengths for the different GCM runs are shown in Figure 9 and Figure 10 for monsoon precipitation and monsoon streamflow, respectively. These ranks are calculated from the distribution of trends in the control runs, which is derived by a Monte Carlo method described in details below. It can be seen that the observed signal strength, considering multimodel ensemble-averaged fingerprint (also true when most of the other GCM fingerprints are considered), lies outside the range expected from natural variability alone at very high statistical confidence (>95%) for both monsoon precipitation and monsoon streamflow, thus achieving "detection."

[32] The significance tests in Figure 9 and Figure 10 are conducted using an ensemble approach which reduces the

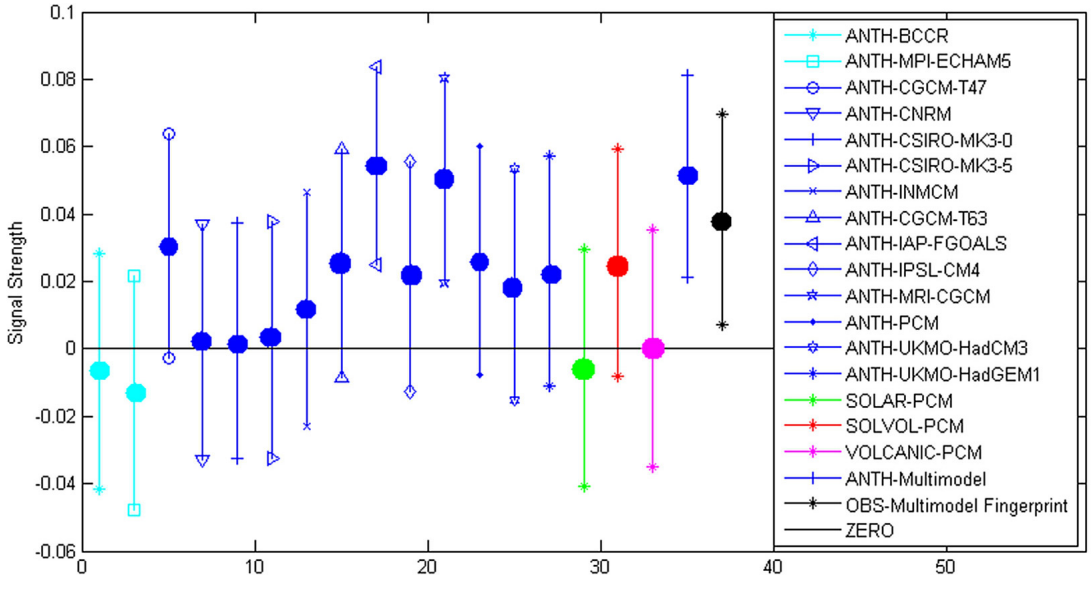

Figure 8. Detection plot for monsoon streamflow. Markings are same as Figure 7.

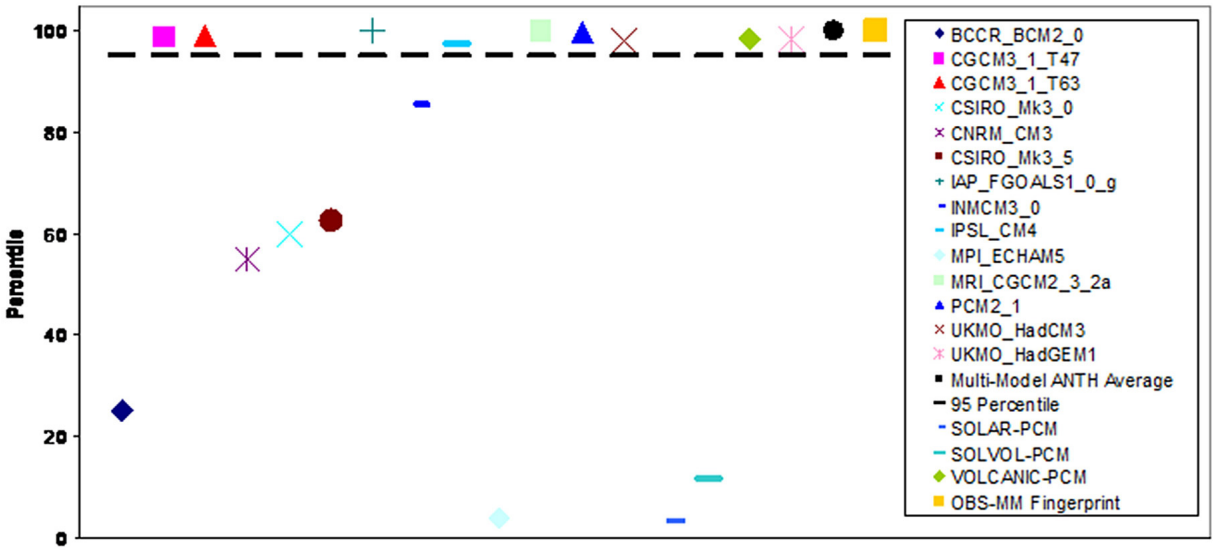

Figure 9. Percentile ranks of ensemble-averaged signal strengths with respect to pooled noise for monsoon precipitation. The 95 percentile from the noise distribution is shown as a dotted line and the signal strengths from the externally forced runs which lie above the line are beyond the range expected from natural internal climate variability. Both the multimodel ensemble-averaged ANTH signal strength and the observed signal strength are found to lie outside the 95% confidence range expected from the control runs.

random "weather noise" [*Barnett et al.*, 2008]. The Monte Carlo method used to estimate the distribution of noise estimates the likelihood that a given ensemble mean value of signal strength, S, can be drawn from the control runs, given an ensemble of k members (for example, $k = 6$ for ANTHpcm, $k = 3$ for SOLpcm, $k = 3$ for VOLCANICpcm and $k = 4$ for SOLVOLpcm, $k = 1$ for Observations, etc.). Pooled noise data set is first estimated by joining $N(t)$ series from control runs of all the GCMs together (Table 1). Pooling of control runs data from all the GCMs is preferred since it gives conservative estimate of noise [*Santer et al.*, 2007].

[33] Groups of k members are now randomly selected from among all the nonoverlapping 49-year segments in the pooled noise and their ensemble-averaged S value is calculated. This is repeated 10,000 times to form a distribution of control S for comparison with forced runs for each model run or the observations. The likelihood that the

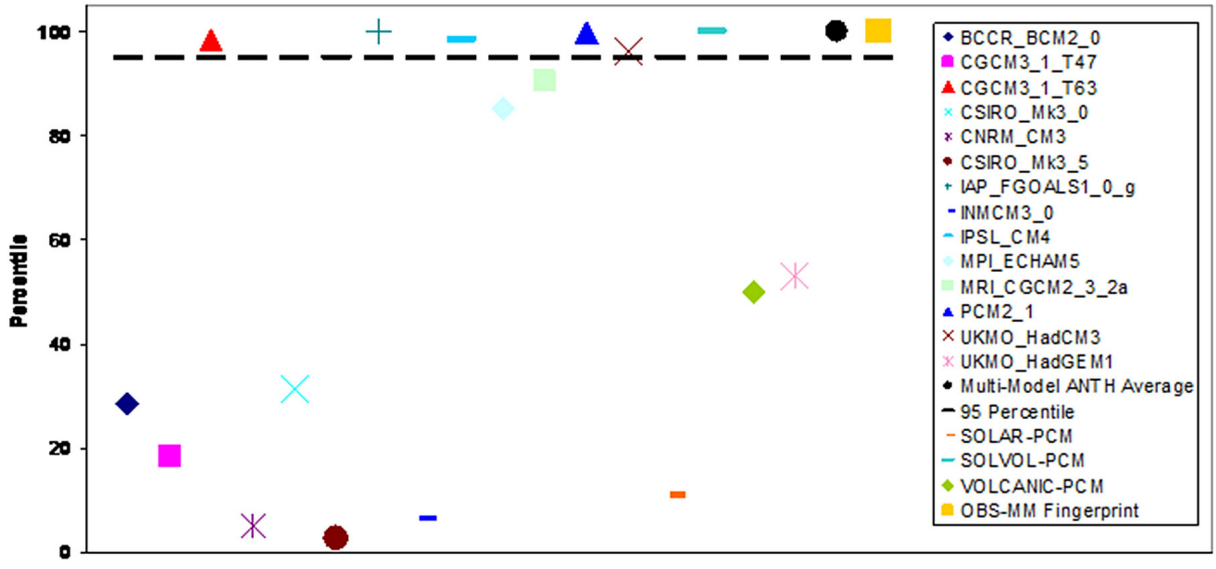

Figure 10. Percentile ranks of ensemble mean signal strengths with respect to pooled noise for monsoon streamflow. Markings are same as Figure 9. For streamflow, too, both the multimodel ensemble-averaged ANTH signal strength and the observed signal strength are found to lie outside the 95% confidence range expected from the control runs.

signal strength corresponding to each model run or the observations falls within the noise distribution is estimated based on their percentile ranks with respect to the noise distribution. As an example, if we consider the ANTH signal strengths of BCCR-BCM2.0 and CGCM3.1-T63 for monsoon precipitation, ensemble size $k = 1$ for each. Hence, one 49-year segment is drawn from the pooled $N(t)$ series and the signal strength is computed. This is repeated 10,000 times.

[34] The probability density functions (pdf) of these signal strengths is shown in Figure 11, along with the positions of the ANTH signal strengths from BCCR-BCM2.0 and CGCM3.1 T63 and the observed signal strength with multimodel ensemble-averaged fingerprint. It is observed that the ANTH signal strength from BCCR-BCM2.0 is more likely to be drawn from the control runs than the ANTH signal strength from CGCM3.1 T63, or the observed signal strength (S_{obs}). Figure 7 and Figure 8 show that the signal strength in the hydrological observations, which cannot be explained by natural internal climate variability alone, is consistent in sign with signal strengths of anthropogenically forced runs of several GCMs (shown in blue). In general, such consistency is more common across GCMs for monsoon streamflow than for monsoon precipitation.

[35] It is argued in recent studies [*Santer et al.*, 2007; *Pierce et al.*, 2009] that multimodel ensemble-averaged estimates perform superior in simulating climate compared to any individual model. One possible reason for this is the reduction in noise because of ensemble-averaging. In this study, too, it has been found that the multimodel ensemble-averaged anthropogenic signal strength is consistent with the observed signal strength for both precipitation and streamflow. The difference in S values between the observation and the multimodel ensemble average anthropogenic run is statistically insignificant for both monsoon precipitation and streamflow. The multimodel ensemble-averaged ANTH signal strength is about 71% of the observed signal strength for monsoon precipitation, which means that about 71% of the trends in monsoon precipitation in the Mahanadi river basin over the second half of the 20th century can be attributed to anthropogenic climate change. The unexplained portion (about 29%) of the trends in monsoon precipitation, on the other hand, can be due to changes in regimes of atmospheric circulation patterns which are not taken into account in the historical GCM runs or because of other local influences. For monsoon streamflow, the multimodel ensemble-averaged ANTH signal is stronger than the observed signal strength. Thus, the multimodel ensemble-averaged anthropogenic climate change estimate is, in some sense, underpredicting the responses in local monsoon precipitation and overpredicting the same in monsoon streamflow for this river basin. The percentage attribution for each GCM is given in Table 2, both for monsoon precipitation and streamflow.

[36] Figure 7 and Figure 8 also give us an idea about the relative merits of each climate model in simulating the hydrological variables in this region of interest. The GCMs shown in cyan (BCCR-BCM2.0, CGCM3.1-T47, CNRM-CM3, CSIRO-Mk3.0, CSIRO-Mk3.5, INM-CM3.0 for monsoon precipitation; BCCR-BCM2.0 and MPI-ECHAM5 for monsoon streamflow) are performing poorly as compared to those shown in blue, since their anthropogenic signal strengths

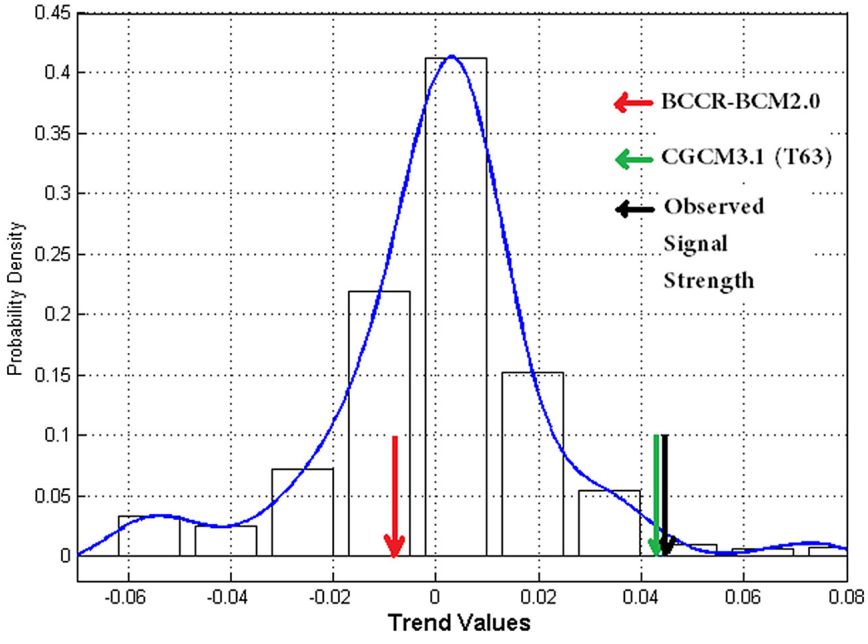

Figure 11. Pdf of trends from the control run, with $k = 1$. The positions of the ANTH signal strengths from BCCR-BCM2.0 and CGCM3.1 (T63) for monsoon precipitation are shown. It can be seen that the probability of finding the ANTH signal strength from BCCR-BCM2.0 in the control runs is much higher than the probability of finding the same from CGCM3.1 (T63). Thus, the ANTH signal strength of BCCR-BCM2.0 is not significantly different from the noise distribution. The observed signal strength with multimodel ensemble-averaged fingerprint for monsoon precipitation is also shown to be unlikely to be found in the control runs.

Table 2. Detection and Attribution Summary at 10% Significance

	Precipitation			Streamflow		
GCM Name	Detection	Year of Detection	Attribution	Detection	Year of Detection	Attribution
BCCR_BCM2_0	✓	1981	X	✓	1974	X
CGCM3_1_T47	✓	1999	X	✓	1974	79%
CGCM3_1_T63	✓	1999	97%	✓	1990	66%
CNRM_CM3	✓	1974	X	✓	1990	5%
CSIRO_MK3_0	X	–	X	✓	1981	6%
CSIRO_MK3_5	X	–	X	✓	1981	7%
IAP_FGOALS1_0_g	✓	1998	100%	X	–	X
INMCM3_0	✓	1998	X	✓	1974	30%
IPSL_CM4	✓	1996	100%	✓	1983	56%
MPI_ECHAM5	✓	1999	25%	✓	1988	X
MRI_CGCM	X	–	X	✓	1974	100%
PCM2_1	✓	1998	62%	✓	1987	68%
UKMO_HadCM3	X	–	X	✓	1989	50%
UKMO_HadGEM1	✓	1998	6%	✓	1987	60%
MultiModel	✓	**1996**	**71%**	✓	**1968**	**100%**

are opposite in sign with the observed signal strength (Figure 7 and Figure 8). A reason for this might be the unrealistic simulation of climate by these GCMs so far as the regional hydrological variables are concerned in the river basin of interest. This is reaffirmed in Figure 9 and Figure 10, which show that the anthropogenically forced signal strengths of these GCMs do not evolve or significantly differ from the preindustrial control runs. An example can be seen in Figure 11 which shows that BCCR-BCM2.0 anthropogenic signal is definitely less realistic as compared to that of CGCM3.1 (T63), for the region and variable of interest. This implies that for the poorer GCMs, the human emissions and the subsequent increase in greenhouse gases in the atmosphere post industrialization might not have been taken into consideration accurately, as far as regional hydrology in this region of interest is concerned. *Hidalgo et al.* [2009] also mention that averaging over relatively small regions often produces a distribution of anthropogenically forced responses that is not well separated from that of natural internal variability.

[37] Among the other plausible natural external climatological causes for the observed hydrological changes, it is interesting to note that the volcanically forced signal strength is also consistent with the observed trends for monsoon precipitation, and both solar and volcanically forced signal strength is also consistent with the observed trends for monsoon streamflow (shown in Figure 7 and Figure 8). However, this observation about natural external forcings is based on outputs from one single GCM. (PCM2.1). It is to be noted that in order to convincingly conclude about observed hydrological changes being explained (or not) by the solar or volcanic activities, we would require data from runs with only these external forcings from several GCMs instead of PCM2.1 alone, which at present is not available from the WCRP/CMIP3 database. *Gillett et al.* [2004] also detected volcanic influence in global precipitation, based on the outputs of PCM2.1 alone.

[38] For estimation of detection times, least squares linear trends of increasing length are fitted to the signal and noise series $N(t)$. However, here, instead of using pooled noise from all the GCMs together, following *Santer et al.* [1994], noise is derived from long preindustrial control runs of each of the individual GCMs separately. In other words, noise and signal from the same GCM are considered. The detection years for both the hydrological variables are also mentioned in Table 2. The time evolutions of signal-to-noise ratio for monsoon precipitation and streamflow are given in Figure 12 and Figure 13, respectively. Figure 12 and Figure 13 also show the 10% significance levels of the signal-to-noise ratio assuming a Gaussian distribution of trends, and detection is achieved when the signal-to-noise ratio stays above this line.

[39] In general, the signal to noise ratios are found to be higher for streamflow as compared to precipitation. It can also be noted that detection of hydrologic change over and above natural internal climate variability is discernible earlier in monsoon streamflow than in monsoon precipitation, across most of the GCMs. *Barnett et al.* [2008] also reported detection of anthropogenic signal in streamflow center timing, while trends in precipitation are indistinguishable from natural variability. In order to understand why the detection and attribution results of precipitation may differ from that of streamflow, it must be kept in mind that while calculating the observed signal strengths (shown in black in Figure 7 and Figure 8), as well as the signal to noise ratios (shown in Figure 12 and Figure 13), year by year dot products are taken between the anthropogenic fingerprint and the observed space-time series of precipitation and streamflow, depending on the variable under consideration. Thus, the difference in trends and variability in the observations of precipitation and streamflow significantly influences the precipitation-streamflow differences in the detection and attribution analysis, in this case, leading to earlier detection times and a stronger signal in streamflow as compared to precipitation. The coefficient of variation (C_v) for observed monsoon streamflow series is 51.436, while for precipitation series, the maximum value of C_v out of the eight locations is 28.801. Variability in the streamflows is likely to be more because it is influenced by land use change and also by climate variables such as temperature, net radiation, relative humidity etc that determine evapotranspiration. The GP based rainfall-runoff model

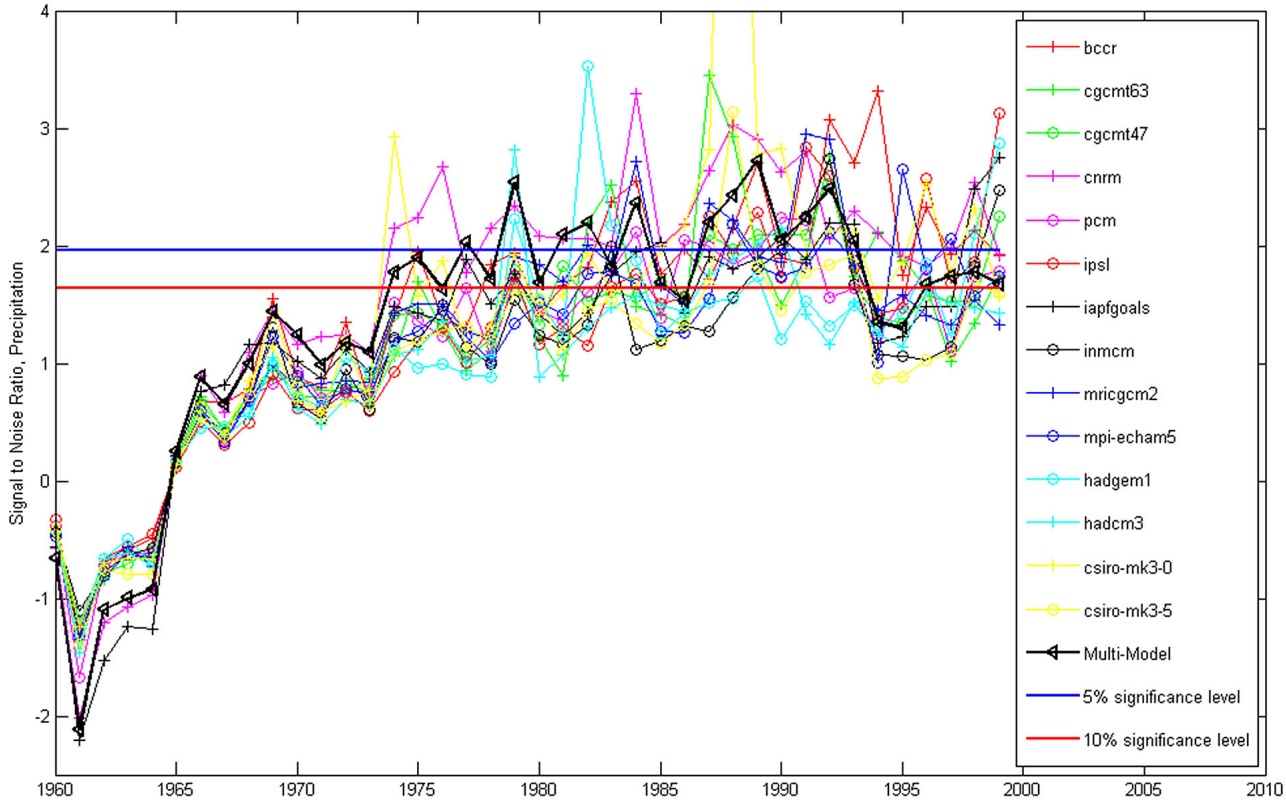

Figure 12. Time-dependent signal to noise estimates for monsoon precipitation. The time-evolution of the signal to noise ratios from the different GCMs and the multimodel ensemble average is shown. The red horizontal line shows the 10% significance level and detection occurs when the signal-to-noise ratio stays above this line.

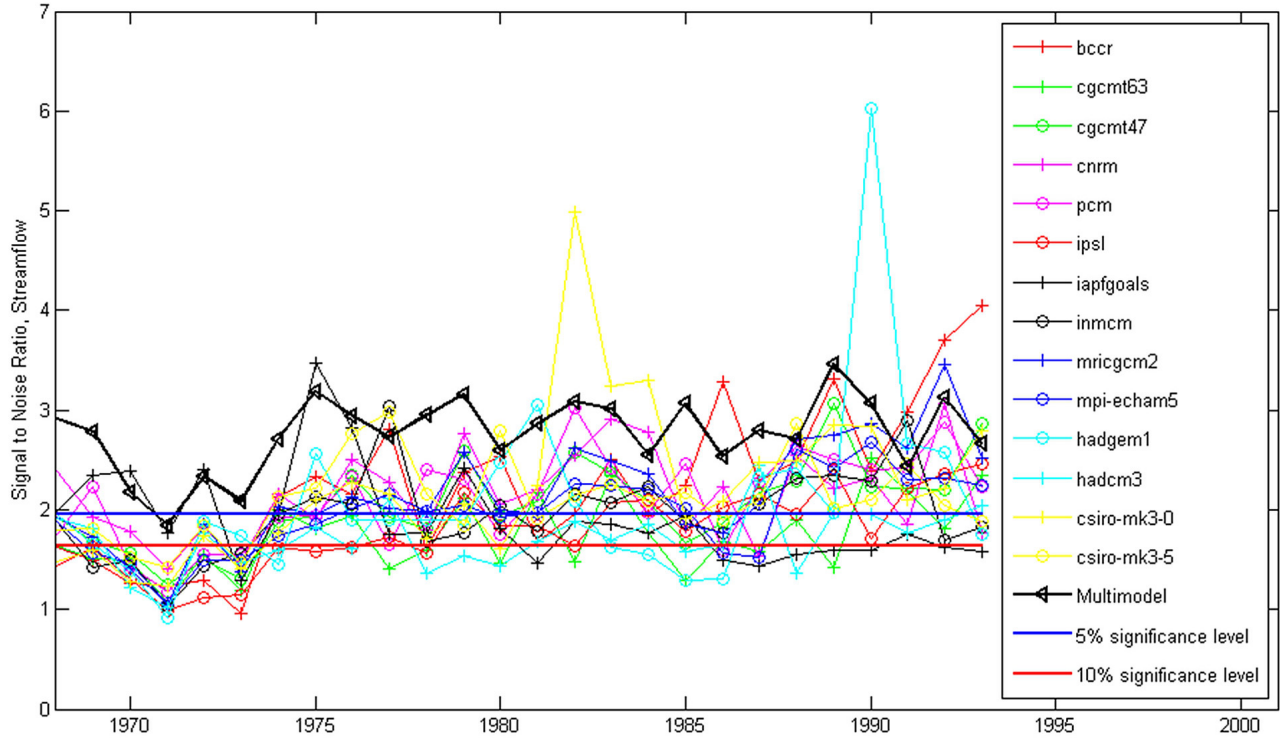

Figure 13. Time-dependent signal to noise estimates for monsoon streamflow. Markings are same as Figure 12.

which is used to derive simulated streamflow corresponding to each GCM run, is assumed to be capable of learning the behavior of the complex intermediate processes converting rainfall to runoff. Although the simulated streamflows are thus deterministically derived, yet this does not guarantee that the variabilities or the trends of the rainfall and the generated streamflow are same, particularly, given the highly nonlinear and complex relation between them.

[40] It is to be noted that the fingerprint-based "detection of climate change" in precipitation or streamflow that is presented here, is different from the commonly perceived "detection of statistical change" in the hydrological time series. "Detection of statistical change" involves parametric and nonparametric methods for detecting significant trends or change points in the hydrologic time series. On the other hand, "detection of climate change" occurs only when the *trends in the hydrological observations lie significantly outside the distribution of trends expected from natural internal variability of climate alone* (estimated from precipitation and streamflow corresponding to no-forcing preindustrial control runs of climate models). It is not unnatural for the observed trend in streamflow to differ from the observed trend in precipitation because of the complex transformation of precipitation into streamflow, and this is what subsequently causes the differences in the climate change detection results between precipitation and streamflow. It should be mentioned that our estimate of natural internal variability of climate, for both precipitation and streamflow, may be uncertain because of stationarity assumption of both the statistical downscaling model and the streamflow generating mechanism. Also, long observed precipitation or streamflow data spanning over centuries including the preindustrial times that would correctly estimate climate noise is unavailable. However, since in this case study, the observed trends in streamflow or precipitation are much higher than the trends expected from climate noise, moderate change in climate noise trend values introduced by use of a physically based model is unlikely to change the D&A analysis results to a great extent. As an example, Figure 11 shows that the mean trend value expected from climate noise is about 0.005, while the observed trend (signal strength) is about 0.045, almost an order of magnitude higher.

[41] The findings of the D&A analysis in monsoon precipitation and streamflow in the Mahanadi river basin is significant in the context of changing climate and the predicted further decrease in future flows in this region reported in other studies [*Mujumdar and Ghosh*, 2008; *Ghosh and Mujumdar*, 2009; *Raje and Mujumdar*, 2010] and hence, it needs to be considered for future water planning and adaptation.

4.1. Limitations of the Study

[42] It is to be noted that the detection and attribution procedure adopted in this study involves uncertainties because of the observed data, the fingerprint method, as well as because of the use of models in order to derive the climate change signal and the noise of natural internal climate variability in the monsoon precipitation and streamflow. Although the observed precipitation and streamflow data are obtained from official government sources that perform quality control exercises on the data, uncertainties in observed records cannot be ruled out completely. The fingerprint based detection and attribution analysis has been applied rarely in regional hydrological applications [*Barnett et al.*, 2008] which are known to have more noise. Additionally, the analysis is forced to rely on models for estimation of climate change signal and natural internal variability noise, in the absence of long observation records prior to and after industrialization. Calibration or verification of the detection analysis is not possible because of absence of any hydrologic or climate reconstructions data set for this river basin. Also, the GCM predictions and their subsequent downscaling to simulate basin-scale precipitation may not be completely accurate because of limitations of our knowledge of the climate system, scale mismatch between GCM grid points and hydrological observation stations and uncertainties in the downscaling model. The GP-based rainfall-runoff model further acts as a source of uncertainty, and our analysis relies on the assumption that the model is capable of learning, at least implicitly, the complex underlying processes that convert rainfall to river flows. The structure of the downscaling model as well as the streamflow generating mechanism is assumed to unchanging over different climate scenarios, which acts as a further limitation of the analysis. Considering several influencing climate variables in the streamflow generation process that affects the intermediate processes converting rainfall to runoff would be more tenable. Addressing data and model uncertainties and fixing the scale and methodological issues can be taken up in future research.

5. Concluding Remarks

[43] A fingerprint-based detection and attribution analysis has been attempted in this study to obtain an insight into the observed changes during the second half of the 20th century in monsoon precipitation and streamflow in the catchment of the Mahanadi River, a tropical rain-fed river draining large coastal areas in eastern India. The fingerprint based detection and attribution analysis employed in this study attempts to isolate the signature of anthropogenically forced changes in the hydrological variables from the historical climate model runs, and to determine how similar the observed changes are to the fingerprint. Thereafter the likelihood of a signal of the observed strength occurring by chance due to natural climate variability alone, as estimated from the long preindustrial control runs, is calculated.

[44] Fourteen climate models are chosen based on availability of predictor data set for all the historical runs used in this study. Statistical downscaling is used to obtain precipitation in the river basin from the large-scale climate variables for each GCM run. A Genetic-Programming based rainfall-runoff model has been used to get corresponding streamflows from the downscaled precipitations.

[45] Using a standard approach that takes into consideration the variability across different climate model simulations, it has been found that the observed trends over the second half of the 20th century in both monsoon precipitation and streamflow lie outside the range expected from natural internal climate variability alone at 95% statistical confidence level for most of the GCMs. However, the observed hydrological changes cannot yet be collectively attributed to human-induced climate change across all the climate models. For some climate models which are found

to simulate the climate more reliably and realistically, the observed hydrological trends are found to be consistent with those predicted by anthropogenic emissions of greenhouse gases. The multimodel ensemble averaged anthropogenic signal strength is found to explain the trends in the observations, for both monsoon precipitation and streamflow. However, changes in observed monsoon precipitation are found to be consistent with those expected from historical volcanic emissions too, while observed monsoon streamflow changes also agree with those expected as a result of both solar and volcanic activities. Detection and attribution of the observed hydrological trends to human-induced climate change is, in general, more conspicuous across the climate models for streamflow as compared to precipitation. Also, detection has been achieved earlier for streamflow than precipitation for most of the GCMs.

[46] The study attempts to formally establish the presence and impacts of human-induced climate change in the observed decreases in monsoon precipitation and streamflow in the Mahanadi river basin. Significant observed hydrological trends above the natural internal variability of climate alone would imply an unlikely restoration of the hydrological cycle to its natural state on its own. This is critical, particularly in the light of the likely increases in dryness and water shortage in the river basin predicted by other recent studies.

[47] It is to be noted, however, that uncertainties because of the detection methodology, data or models used may affect the findings of the analysis. Though GCMs are the most credible tools at present to study regional impacts of climate change on natural systems, they may not capture local-scale features like land-use changes. The statistical downscaling and subsequent rainfall-runoff model provide only the present best approximation to simulate regional hydrological features, subject to observational and modeling constraints.

[48] The detection and attribution analysis presented in this work for river basin–scale hydrological variables can be further extended to consider the effects of nonclimatic localized influences like land-use and land-cover changes, changes in irrigation practices, urbanization etc. This can be achieved by an end-to-end attribution approach where the interface between climate and nonclimate models is explicitly modeled [*Stone and Allen*, 2005; *Zwiers and Hegerl*, 2008; *Stone et al.*, 2009]. Modifications in the D&A methodology to address uncertainties can also be attempted in future studies.

Appendix A: Principal Component Analysis and Linear Regression Based Downscaling Model

[49] Statistical downscaling techniques are tools to generate synthetic weather data required for regional climate change impact assessment studies from large-scale atmospheric variables. They are extensively being used in studies on climate change impacts on local hydrology in the recent past, since the large-scale outputs of GCMs cannot directly be used in any regional hydrologic model of interest [*Wigley et al.*, 1990; *Carter et al.*, 1994]. Statistical downscaling techniques essentially form a predictor-predictand relationship between the large-scale climate variables and the regional- or local-scale meteorological/hydrological variables.

[50] The most popular approach of downscaling is the use of a transfer function which is a regression based downscaling method [*Crane and Hewitson*, 1998; *Wilby et al.*, 1998, 2002; *Ghosh and Mujumdar*, 2008], that relies on direct quantitative relationship between the local-scale variable (predictand) and the variables containing the large-scale climate information (predictors) through some form of regression. In this study, per *Ghosh and Mujumdar* [2006], a principal component analysis and linear regression model is used to downscale the GCM outputs for estimation of monthly rainfall at the eight rainfall locations. Appropriate seasonal component is added to the regression model for improving the goodness of fit.

[51] Precipitation is linked to air mass transport and atmospheric water content and thus can be related to atmospheric circulation or pressure patterns, specific humidity and temperature. Hence, near surface air temperature, mean sea level pressure, specific humidity at 850 hPa and geopotential height at 500 hPa are selected as predictors for the downscaling model. Apart from being physically meaningful, these predictors are reasonably well simulated by the GCMs, and are available for many control runs and historical runs of the GCMs used in this study. In absence of observed climate variables, as per standard practice, monthly data of these predictors for a region extending from 15°N to 25°N and 80°E to 90°E are obtained from the National Centers for Environmental Prediction/National Center for Atmospheric Research (NCEP/NCAR) reanalysis data for the years 1951–1999 [*Kalnay et al.*, 1996] (available online at: http://www.cdc.noaa.gov/cdc/data.ncep.reanalysis.html) and are used for training the model, with the observed monthly precipitation as the predictand. Large-scale monthly atmospheric variables output from the different GCM runs are extracted from the multiple model data set of WCRP/CMIP3 (see https://esg.llnl.gov:8443/about/ftp.do). Principal component analysis is done following bias removal and normalization [*Ghosh and Mujumdar*, 2008], on the NCEP data to identify the patterns of multidimensional variables and to transfer correlated variables into a set of uncorrelated variables. The regression equations are now fit between the first 10 principal components (which explains 99% of the overall variance) of the predictor data set and the observed precipitation at each of the eight locations. All the coefficients used in the regression equations are rewritten in terms of seasonal component which is assumed to be different for different months with a periodicity of 12.

[52] Thus, precipitation P_t at time step t is given by [*Ghosh and Mujumdar*, 2006]

$$P_t = C + \sum_{k=1}^{K} \beta_k \times pc_{kt}, \tag{A1}$$

where pc_{kt} is the kth principal component of the predictor data set in time t, and C and β_k are the regression coefficients, K (=10) is the number of principal components. In terms of the seasonal components,

$$C = C^0 + C^1 \times \sin(2\pi p/12) + C^2 \times \cos(2\pi p/12), \tag{A2}$$

$$\beta_k = \beta_k^0 + \beta_k^1 \times \sin(2\pi p/12) + \beta_k^2 \times \cos(2\pi p/12), \tag{A3}$$

where p is the serial number of the month within a year ($p = 1, 2, 3, \ldots, 12$), corresponding to time period t of equation (A1). Insignificant coefficients (in terms of the t statistic p value) are removed from the model without loss in the R value. The residuals, after relevant statistical tests, are found to be independent and identically distributed following the normal distribution.

[53] Additionally, fuzzy clustering is performed on the predictor data set and the fuzzy memberships are used as input in the regression model. However, since no significant improvement is noticed in the correlation coefficient for the testing data set, fuzzy clustering is dropped from the downscaling methodology.

[54] The coefficient matrix from the NCEP data and the regression parameters are supplied to standardized and normalized predictor data set from the different GCM runs, interpolated at the NCEP grid points by Mercator projections (conformal cylindrical map projections), to yield downscaled monthly precipitations at the eight locations corresponding to each GCM run.

Appendix B: Genetic Programming Based Rainfall-Runoff Model

[55] Genetic-Programming (GP) is an evolutionary algorithm based model with the unique ability of optimizing both the structure of the model and its parameters. In GP, a computer program, representing the model, relating the output to the input variables is evolved across generations until it represents the best estimate of the model. *Koza* [1992] defines GP as a domain independent problem-solving approach in which computer programs are evolved to solve, or approximately solve, problems based on the Darwinian principles of reproduction and "survival of the fittest."

[56] In principle, GP is the application of Genetic Algorithms (GA) [*Goldberg*, 1989] to a population of computer programs. However, unlike GA, GP works on parse trees instead of bit strings. A parse tree consists of a terminal set (the variables in the problem) and a function set (the basic operators used to form the function). GP first creates a randomly generated population of parse trees. Fitness measure of an individual tree is calculated based on how well it solves the given problem. Subsequently, fit parse trees are selected for reproduction and variation to form a new population or parse trees. Selection, crossover and mutation operations in GP are similar to those of GA functionally. This process is continued until a preset stopping criterion is met.

[57] The implementation of GP to predict monthly inflows to the Hirakud dam from the monthly rainfall in the 5 locations (Location 4—21.5°N, 81.5°E, Location 5—21.5°N, 82.5°E, Location 6—21.5°N, 83.5°E, Location 7—22.5°N, 82.5°E, and Location 8—22.5°N, 83.5°E) that contribute directly to the unregulated inflows to the Hirakud reservoir, is done through the MATLAB GP toolbox GPTIPS1.0 (which is an open source toolbox available at http://gptips.sourceforge.net/as). The population size chosen is 200, and the maximum number of generations is set to 500. Multigene symbolic regression fitness function is used, which minimizes the root mean square error (RMSE) between the output and the predicted output, which means that the weights for the genes are obtained using ordinary least squares to regress the genes against the output data. The maximum depth of the trees is chosen as 15 nodes. From the observed data, it is noticed that nonmonsoon flows are extremely insignificant in comparison to the monsoon months flows. Thus there is no additional need to take groundwater base flow into consideration. The variability in streamflow, even if there is no change in precipitation, is taken into consideration by training the model with observed real-time streamflows, and thus, all the factors contributing to generation of streamflow from precipitation are implicitly incorporated into the model.

[58] **Acknowledgments.** The authors sincerely thank David Pierce (Scripps Institution of Oceanography, La Jolla, CA) for helpful discussions through email, and the four anonymous reviewers and the Associate Editor, for reviewing the manuscript and providing critical comments to improve the paper.

References

Allen, M. R., and P. A. Stott (2003), Estimating signal amplitudes in optical fingerprinting, part I: theory, *Clim. Dyn.*, *21*, 477–491.

Allen, M. R., and S. F. B. Tett (1999), Checking for model consistency in optimal fingerprinting, *Clim. Dyn.*, *15*, 419–434.

Babovic, V., and M. Keijzer (2006), Rainfall-runoff modeling based on genetic programming, in *Encyclopedia of Hydrological Sciences*, Wiley, New York, doi:10.1002/0470848944.

Barnett, T. P., D. W. Pierce, and R. Schnur (2001), Detection of anthropogenic climate change in the world's oceans, *Science*, *292*, 270–274.

Barnett, T. P., D. W. Pierce, K. M. AchutaRao, P. J. Gleckler, B. D. Santer, J. M. Gregory, and W. M. Washington (2005), Penetration of human-induced warming into the world's oceans, *Science*, *309*, 284–287.

Barnett, T. P., et al. (2008), Human-induced changes in the hydrology of the western U.S., *Science*, *319*, 1080–1083.

Bonfils, C., et al. (2008), Detection and attribution of temperature changes in the mountainous western United States, *J. Clim.*, *21*, 6404–6424.

Carter, T. R., M. L. Parry, H. Harasawa, and S. Nishioka (1994), *IPCC Technical Guidelines for Assessing Climate Change Impacts and Adaptations*, Univ. College, London.

Cavazos, T., and B. C. Hewitson (2005), Performance of NCEP variables in statistical downscaling of daily precipitation, *Clim. Res.*, *28*, 95–107.

Crane, R. G., and B. C. Hewitson (1998), Doubled CO_2 precipitation changes for the Susquehanna basin: Downscaling from the GENESIS general circulation model, *J. Climatol.*, *18*, 65–76.

Dorado, J., J. R. Rabunal, A. Pazos, D. Rivero, A. Santos, and J. Puertas (2003), Prediction and modeling of the rainfall–runoff transformation of a typical urban basin using ANN and GP, *Appl. Artif. Intell.*, *17*, 329–343.

Gedney, N., P. M. Cox, R. A. Betts, O. Boucher, C. Huntingford, and P. A. Stott (2006), Detection of a direct carbon dioxide effect in continental river runoff records, *Nature*, *439*, 835–838.

Ghosh, S., and P. P. Mujumdar (2006), Future rainfall scenario over Orissa with GCM projections by statistical downscaling, *Curr. Sci.*, *90*, *3*, 396–404.

Ghosh, S., and P. P. Mujumdar (2007), Nonparametric methods for modeling GCM and scenario uncertainty in drought assessment, *Water Resour. Res.*, *43*, W07405, doi:10.1029/2006WR005351.

Ghosh, S., and P. P. Mujumdar (2008), Statistical downscaling of GCM simulations to streamflow using relevance vector machine, *Adv. Water Resour.*, *31*(1), 132–146.

Ghosh, S., and P. P. Mujumdar (2009), Climate change impact assessment-uncertainty modeling with imprecise probability, *J. Geophy. Res.*, *114*, D18113.

Gillett, N. P., F. W. Zwiers, A. J. Weaver, and P. A. Stott (2003), Detection of human influence on sea-level pressure, *Nature*, *448*, 461–465, doi:10.1038/nature01487.

Gillett, N. P., A. J. Weaver, F. W. Zwiers, and M. F. Wehner (2004), Detection of volcanic influence on global precipitation, *Geophys. Res. Lett.*, *31*, L12217, doi:10.1029/2004GL020044.

Goldberg, D. E. (1989), *Genetic Algorithms for Search, Optimization and Machine Learning*, Addison-Wesley Publ., Reading, Mass.

Hasselmann, K. (1979), On the signal-to-noise problem in atmospheric response studies, in *Meteorology Over the Tropical Oceans*, edited by B. D. Shaw, pp. 251–259, R. Meteorol. Soc., Bracknell, U.K.

Hawkins, E., and R. Sutton (2012), Time of emergence of climate signals, *Geophy. Res. Lett.*, *39*, L01702.

Hegerl, G. C., and F. W. Zwiers (2011), Use of models in detection and attribution of climate change, *Clim. Change*, *2*, 570–591.

Hegerl, G. C., H. von Storch, K. Hasselmann, B. D. Santer, U. Cubasch, and P. D. Jones (1996), Detecting greenhouse-gas induced climate change with an optimal fingerprint method, *J. Clim.*, *9*, 2281–2306.

Hidalgo, H. G., et al. (2009), Detection and attribution of streamflow timing changes to climate change in the western United States, *J. Clim.*, *22*, 3838–3855.

Intergovernmental Panel on Climate Change (2010), Meeting report of the Intergovernmental Panel on climate change expert meeting on detection and attribution related to anthropogenic climate change, report, pp. 55, IPCC Working Group I Technical Support Unit, Univ. of Bern, Bern, Switzerland.

Jain, A., and Kumar, S. (2009), Dissection of trained neural network hydrologic model architectures for knowledge extraction, *Water Resour. Res.*, *45*, W07420, doi:10.1029/2008WR007194.

Jain, S. K., P. C. Nayak, and K. P. Sudheer (2008), Models for estimating evapotranspiration using artificial neural network and their physical interpretation, *Hydrol. Processes*, *22*(13), 2225–2234.

Jayawardena, A. W., N. Muttil, and T. M. K. G. Fernando (2005), Rainfall-Runoff modeling using Genetic Programming, in *MODSIM 2005 International Congress on Modeling and Simulation*, edited by A. Zerger and R. M. Argent, pp. 1841–1847, Model. and Simul. Soc. of Aust. and N.Z., Canberra, Australia.

Jones, P. D., and G. C. Hegerl (1998), Comparisons of two methods of removing anthropogenic-related variability from the near-surface observational temperature field, *J. Geophys. Res.*, *103*, 13,777–13,786.

Kalnay, E., et al. (1996), The NCEP/NCAR 40-year reanalysis project, *Bull. Am. Meteorol. Soc.*, *77*, 437–471, doi:10.1175/1520-0477.

Karoly, D. J., and Q. Wu (2005), Detection of regional surface temperature trends, *J. Clim.*, *18*, 4337–4343.

Kashid, S., S. Ghosh, and R. Maity (2010), Streamflow prediction using multi-site rainfall obtained from hydroclimatic teleconnection, *J. Hydrol.*, *395*, 23–38, doi:10.1016/j.jhydrol.2010.10.004.

Koza, J. (1992), *Genetic Programming: On the Programming of Computers by Natural Selection*, MIT Press, Cambridge, Mass.

Liong, S. Y., T. R. Gautam, S. T. Khu, V. Babovic, and N. Muttil (2002), Genetic programming: A new paradigm in rainfall-runoff modeling, *J. Am. Water Res. Assoc.*, *38*(3), 705–718.

Maurer, E. P., I. T. Stewart, C. Bonfils, P. B. Duffy, and D. R. Cayan (2007), Detection, attribution, and sensitivity of trends toward earlier streamflow in the Sierra Nevada, *J. Geophys. Res.*, *112*, D11118, doi:10.1029/2006JD008088.

Min, S. K., X. Zhang, F. W. Zwiers, and G. C. Hegerl, (2011), Human contribution to more-intense precipitation extremes, *Nature*, *470*, 378–381, doi:10.1038/nature09763.

Mohapatra, M., and U. C. Mohanty (2006), Spatio-temporal variability of summer monsoon rainfall over Orissa in relation to low pressure systems, *J. Earth Syst. Sci.*, *115*, *2*, 203–218.

Mujumdar, P. P., and S. Ghosh (2008), Modeling GCM and scenario uncertainty using a possibilistic approach: Application to the Mahanadi River, India, *Water Resour. Res.*, *44*, W06407, doi:10.1029/2007WR006137.

Muttil, N., and S. Y. Liong (2001), Improving runoff forecasting by input variable selection in genetic programming, in *Proc. ASCE World Water Congress*, vol. 111, p. 76, Am. Soc. of Civil Eng., Orlando, Fl. doi:10.1061/40569(2001)76.

Parthasarathy, B., A. A. Munot, and D. R. Kothawale (1995), Monthly and seasonal rainfall series for all India homogeneous regions and meteorological subdivisions: 1871–1994, *Res. Rep. RR-065*, Indian Inst. of Trop. Meteorol., Pune, India.

Patri S. (1993), Data on flood control operation of Hirakud dam, report, Dept. of Irrigation, Gov. of Orissa, India.

Pierce, D. W., et al. (2008), Attribution of declining western U.S. snowpack to human effects, *J. Clim.*, *21*, 6425–6444.

Pierce, D. W., T. P. Barnett, B. D. Santer and P. J. Gleckler (2009), Selecting global climate models for regional climate change studies, *Proc. Natl. Acad. Sci. USA*, *106*, 8441–8446.

Raje, D. and P. P. Mujumdar (2009), A conditional random field based downscaling method for assessment of climate change impact on multisite daily precipitation in the Mahanadi basin, *Water Resour. Res.*, *45*, W10404, doi:10.1029/2008WR007487.

Raje, D., and P. P. Mujumdar (2010), Constraining uncertainty in regional hydrologic impacts of climate change: Nonstationarity in downscaling, *Water Resour. Res.*, *46*, W07543, doi:10.1029/2009WR008425.

Rao, P. G. (1995), Effect of climate change on streamflows in the Mahanadi river basin, India, *Water Int.*, *20*, 205–212.

Rao, P. G., and K. K. Kumar (1992), Climatic shifts over Mahanadi river basin, *Curr. Sci.*, *63*, 192–196.

Rodríguez-Vázquez, K., M. L. Arganis Juárez, C. C. Villanueva, and R. Domínguez-Mora (2012), Rainfall–runoff modeling using genetic programming, *J. Hydroinformatics*, *14*, 108–121, doi:10.2166/hydro.2011.105.

Santer, B. D., W. Bruggemann, U. Cubasch, K. Hasselmann, E. Maier-Reimer, and U. Mikolajewicz (1994), Signal-to-noise analysis of time-dependent greenhouse warming experiments. Part 1: Pattern analysis, *Clim. Dyn.*, *9*, 267–285.

Santer, B. D., U. Mikolajewicz, W. Bruggemann, U. Cubasch, K. Hasselmann, H. Hock, E. Maier-Reimer and T. M. L. Wigley (1995), Ocean variability and its influence on the detectability of greenhouse warming signals, *J Geophy. Res.*, *100*, 10,693–10,725.

Santer, B. D., et al. (2007), Identification of human induced changes in atmospheric moisture content, *Proc. Natl. Acad. Sci. USA*, *104*, 15,248–15,253.

Savic, D. A., G. A. Walters, and G. W. Davidson (1999), A genetic programming approach to rainfall-runoff modeling, *Water Resour. Manage.*, *13*, 219–231.

Stone, D. A., and M. R. Allen (2005), Attribution of global surface warming without dynamical models, *Geophys. Res. Lett.*, *32*, L18711, doi:10.1029/2005GL023682.

Stone, D. A., M. R. Allen, P. A. Stott, P. Pall, S. K. Min, T. Nozawa, and S. Yukimoto (2009), The detection and attribution of human influence on climate, *Ann. Rev. Environ. Resour.*, *34*, 1–16.

Stott, P. A., N. P. Gillett, G. C. Hegerl, D. J. Karoly, D. A. Stone, X. Zhang, and F. W. Zwiers (2010), Detection and attribution of climate change: A regional perspective, *Wiley Interdiscip. Rev. Clim. Change*, *1*, 192–211, doi:10.1002/wcc.34.

Sudheer, K. P., and A. Jain (2009), Recent advances in knowledge extraction from artificial neural network based hydrologic models, *ISH J. Hydraul. Eng.*, *15*(1), 75–83.

Timbal, B., J. Arblaster, and S. Power (2006), Attribution of the late 20th century rainfall decline in South-West Australia, *J. Clim.*, *19*, 2046–2062.

Wang, G., J. Xia, and J. Chen (2009), Quantification of effects of climate variations and human activities on runoff by a monthly water balance model: A case study of the Chaobai River basin in northern China, *Water Resour. Res.*, *45*, W00A11, doi:10.1029/2007WR006768.

Whigham, P. A., and P. F. Crapper (2001), Modeling rainfall-runoff relationships using Genetic Programming, *Math. Comput. Model.*, *33*, 707–721.

Wigley, T. M. L., P. D. Jones, K. R. Briffa, and G. Smith (1990), Obtaining subgrid-scale information from coarse-resolution general circulation model output, *J. Geophys. Res.*, *95*, 1943–1953.

Wilby, R. L., H. Hassan, and K. Hanaki (1998), Statistical downscaling of hydrometeorological variables using general circulation model output, *J. Hydrol.*, *205*, 1–19.

Wilby, R. L., C. W. Dawson, and E. M. Barrow (2002), SDSM—A decision support tool for the assessment of regional climate change impacts, *Environ. Modell. Softw.*, *17*, 147–159.

Willett, K. M., N. P. Gillett, P. D. Jones and P. P. Thorne, (2007), Attribution of observed surface humidity changes to human influence, *Nature*, *449*(7163), 710–712, doi:10.1038/nature06207.

Zhang, X., F. W. Zwiers, G. C. Hegerl, F. H. Lambert, N. P. Gillett, S. Solomon, and T. Nozawa (2007), Detection of human influence on twentieth-century precipitation trends, *Nature*, *448*, 461–465, doi:10.1038/nature06025.

Zwiers, F. W., and G. C. Hegerl (2008), Attributing cause and effect, *Nature*, *453*, 296–297.